Enhanced understanding of dominant drivers of Water Yield change across China through the improved coupled carbon and water model

Huilan Shen [1, 2], Hanbo Yang [1, 2, *], Changming Li [1,2,3]

[1] Department of Hydraulic Engineering, Tsinghua University, Beijing 100084, China

[2] State Key Laboratory of Hydroscience and Engineering, Tsinghua University, Beijing 100084, China

[3] School of Civil Engineering and Transportation, State Key Laboratory of Subtropical Building and Urban Science, South China University of Technology, Guangzhou 510641, China

* Correspondence: Hanbo Yang (yanghanbo@tsinghua.edu.cn)

Abstract: The rapid environmental changes, including climate change, escalating atmospheric CO_2 concentration ([CO_2]), and vegetation dynamics, have been significantly impacting hydrological processes. Yet disentangling the respective contributions of climate, vegetation, and [CO2] change to water yield (WY)—especially clarifying [CO2]-driven physiological effects—remains difficult. ~~Accurately quantifying their contribution to water yield (WY) has become a significant challenge in water resource management and climate adaptation studies.~~ Therefore, this study improved the coupled carbon and water (CCW) model integrating dynamic water use efficiency (WUE) better capture CO_2-physiological feedbacks. ~~to quantify the CO_2-physiological feedback~~; Using scenario analysis, WY changes across China from 1982 to 2017 were attributed to climate, vegetation, and [CO_2] drivers. ~~furthermore systematically investigated the causes for WY change during 1982-2017 in China using a scenario analysis method based on the improved CCW model.~~ The results showed that ~~the effects on WY from changes in climate, vegetation, and [CO_2] exhibited a significant regional variability. C~~climate change (especially precipitation change) emerged as the dominant driver, directly affecting over 70% of China's land area. The vegetation change was the second largest factor to reduce WY, especially in central China~~, where vegetation change led to a general decrease in runoff~~. The effect of the escalating [CO_2]~~, which reduced transpiration by inducing stomatal closure,~~ was relatively small. Spatial analysis aligned with isohyetal lines further revealed that vegetation change and [CO_2] exerted greater influence within the 400–1600 mm precipitation range. In addition, the elasticity analysis showed that the sensitivity ranking of impact factors is precipitation ~~($\varepsilon P = 1.55$)~~ > [CO_2] ~~($\varepsilon CO_2 = 0.55$)~~ > NDVI ~~($\varepsilon NDVI = -0.44$)~~ for the whole China. ~~Historically, NDVI change has exceeded precipitation and [CO_2] impacts on runoff in some regions due to its higher relative change; however,~~Therefore, CMIP6 SSP585 projections indicate that accelerating [CO_2] rise ~~(2.34% yr^{-1})~~ will amplify its hydrological effect to a +1.29% annual WY increase by 2100, surpassing vegetation influences. This study refines WY attribution by

coupling dynamic WUE with ecohydrological modeling, valuable insights for optimizing regional water resource allocation and developing adaptive ecosystem management strategies under future climate scenarios. ~~This study provided theoretical support for water resource management and offered new perspectives for climate change adaptation strategies, vegetation restoration, and water resource management.~~

Keywords: the coupled carbon and water (CCW) model; ~~runoff~~ WY change; climate change; vegetation change; increasing atmospheric CO_2 concentrations; attribution analysis

Plain language: Climate change, rising CO_2, and vegetation dynamics are reshaping global water cycle, but their impacts remain unclear. We improved the coupled carbon and water model to analyze China's water yield (WY) changes (1982–2017). Our results showed that climate change was the dominant driver nationally, vegetation/ CO_2 most affected in 400-1600 mm precipitation zones. Projections indicate CO_2 may increase WY 1.3% annually by 2100, surpassing other drivers. This work informs sustainable water management.

1 Introduction

The global environment has been undergoing rapid changes, impacting hydrological processes through climate change, escalating atmospheric CO_2 concentration [CO_2], and vegetation dynamics (Piao et al., 2007; Wei et al., 2024). Notably, China has experienced a visible greening trend in recent decades, prompting a heightened focus on ecological and water resource concerns (Chen et al., 2019). Investigating the influence of vegetation changes on runoff has thus emerged as a pivotal research area, aligning with China's increasing emphasis on environmental sustainability. China's diverse climatic zones and pronounced greening make it an ideal natural laboratory for investigating these ecohydrological feedbacks, with insights that are globally relevant yet directly informative for sustainable water resource management and ecological restoration in China(Ogutu et al., 2021; Yang et al., 2019), ~~,~~ and for other semi-arid and monsoon-influenced regions such as the Sahel, South Asia, and the Mediterranean Basin(Nkiaka et al., 2025; Rahman et al., 2025; Serrano-Notivoli et al., 2022). Understanding the intricate interplay among vegetation dynamics, climate change, and [CO_2] within the water cycle, particularly concerning runoff therefore it is not only of global relevance but also of profound importance for advancing sustainable water resource management and ecological restoration strategies in China under accelerating environmental change~~, holds significant promise for informing future water resource management strategies and ecosystem preservation initiatives and offering valuable insights for climate change adaptation endeavors (Ogutu et al., 2021; Yang et al., 2019).~~

~~Climate change directly affects runoff by altering precipitation patterns, temperature regimes, and radiation levels (Ban et al., 2023; Li et al., 2022). It also indirectly influences runoff dynamics by altering vegetation phenology (Liu et al., 2024). Vegetation, in turn, plays a key role in the hydrological cycle by influencing root water uptake, canopy transpiration, rainfall interception, and soil infiltration processes (Hoek Van Dijke et al., 2022; Shi et al., 2022; Yang et al., 2023; Zhang et al., 2022a).~~

~~Additionally, rising [CO_2] affects transpiration by influencing vegetation photosynthesis, thus indirectly impacting hydrological processes (Wei et al., 2024; Zhou et al., 2023). (Lammertsma et al., 2011; Xu et al., 2016) (Montibeller et al., 2022) Although recent studies have attempted to separate the impacts of vegetation from climate using ecohydrological models, the results remain inconsistent (Fu et al., 2023; Yang et al., 2020). Some research suggested that climate change had a more significant direct impact on runoff (Liu et al., 2024; Yang et al., 2021; Zhai and Tao, 2017, 2021), while others highlighted the comparable or even dominant role of vegetation change and [CO_2] in runoff dynamics (Li et al., 2020b; Wang et al., 2021; Zhou et al., 2023). Therefore, further research is needed to disentangle the complex effects of climate, vegetation, and [CO_2] change on runoff.~~

Several methods have been employed to separate the effects of climate, vegetation, and [CO_2] change on runoff change, including paired catchment experiments, statistical methods, and modeling approaches (Zeng et al., 2020). Given that annual water yield (WY) equates to runoff through negligible soil water storage changes, these methodological evaluations directly inform WY attribution frameworks (Zhang et al., 2022b). The paired catchment experiment method, though classical, is limited to small-scale watersheds and is less applicable to larger regions (Peng et al., 2016). Statistical methods, while helpful in identifying correlations, lack a physical basis and are insufficient for explaining the underlying mechanisms of runoff changes (Chen et al., 2022). Modeling approaches for attribution fall into two broad classes: (i) process-based models that explicitly simulate coupled water–energy–carbon processes, and (ii) conceptual models that approximate these processes with parsimonious, physically interpretable relationships ~~Modeling approaches, which are broadly categorized into conventional hydrological models and ecohydrological models, provide a more systematic framework for attribution analysis. Conventional hydrological models tend to focus on runoff simulation and often oversimplify the effects of vegetation and [CO_2], potentially underestimating their impacts on runoff~~ (Zhai and Tao, 2021). Process-

based models can capture detailed mechanisms, but they require extensive inputs and many parameters, are sensitive to calibration and equifinality, and are computationally demanding—limitations that hinder basin-to-continental applications over long periods(Jiao et al., 2017; Ma et al., 2023).~~Ecohydrological models, which consider both hydrological and vegetation processes, can better separate the effects of climate, vegetation, and [CO_2], but are often computationally demanding and limited in their spatial applicability (Jiao et al., 2017; Ma et al., 2023).~~ By contrast, conceptual models retain key ecohydrological mechanisms with far fewer parameters, scale well to large regions, and thus are well suited for large-scale attribution while preserving physical interpretability. Among these conceptual models ~~modeling approaches~~, the Budyko framework, widely used to separate climate change effects on runoff, quantifies water balance through the aridity index (PET/precipitation) and incorporates a catchment-specific parameter "n" representing integrated land surface characteristics (e.g., vegetation, soil, topography) (Zhang et al., 2022a, 2016a). However, most Budyko-based applications primarily emphasize climate-driven attribution; vegetation and [CO_2] influences are typically introduced only indirectly—by assigning temporal changes in "n" to vegetation(Tan et al., 2024; Xue et al., 2022; Zhou et al., 2023) or correlating "n" with NDVI (Liu et al., 2024; Tan et al., 2023), and by embedding [CO_2] effects through PET adjustments(Liu et al., 2024).~~However, existing studies typically attributed temporal changes in "n" solely to vegetation change (Tan et al., 2024; Xue et al., 2022; Zhou et al., 2023) or correlated "n" with vegetation indices (e.g., NDVI) through multivariate regression (Liu et al., 2024; Tan et al., 2023) (Liu et al., 2024).~~ These practices conflate vegetation with other controls captured by "n" (e.g., soil, topography) and mix [CO_2]-physiological impacts with meteorological drivers in PET, making it difficult to isolate vegetation structural change from [CO_2]-induced stomatal adjustments and to ascribe mechanisms robustly ~~might not accurately reflect the true impact of vegetation change. This is because the approach oversimplifies the role of "n" by conflating vegetation effects with confounding factors (e.g., CO_2-induced stomatal~~

~~adjustments, and climate change), as regression-based methods inherently fail to disentangle covarying drivers, thereby obscuring whether "n" changes originate from vegetation dynamics, CO_2-physiological feedbacks, or multi-factor synergies~~ (Gan et al., 2021). ~~While some studies incorporated [CO_2] effects via PET adjustments instead of actual evapotranspiration, this indirect approach conflates CO_2-driven PET changes with other meteorological drivers (e.g., radiation, wind) and propagates parameter uncertainties (e.g., "n"), obscuring [CO_2]'s independent impact on runoff (Liu et al., 2024).~~

Specifically, elevated [CO_2] reduces stomatal conductance—due to smaller stomatal apertures and increased leaf resistance (Lammertsma et al., 2011; Xu et al., 2016) which decreases transpiration fluxes (ET). At the same time, carbon assimilation rate (GPP) may increase with higher [CO_2] availability, but this increase is often less proportional to the reduction in water loss (Montibeller et al., 2022) The resulting imbalance—lower water loss relative to carbon gain—thus leads to higher water-use efficiency (WUE = GPP / ET). In particular, conventional frameworks that neglect [CO_2]-driven physiological feedbacks fail to represent the enhanced water-use efficiency (WUE) of vegetation under elevated [CO_2] conditions. This omission leads to ambiguous attribution of runoff variations, as part of the reduction in evapotranspiration induced by stomatal closure is often misinterpreted as a vegetation structural effect rather than a [CO_2]-induced physiological adjustment. Although numerous studies have examined vegetation and climate controls on runoff, few have explicitly incorporated the [CO_2]–WUE feedback within a mechanistic framework. Most existing approaches either completely ignore this feedback or treat it as a simple empirical or linear relationship, rather than capturing its process-based influence on hydrological responses.

The coupled carbon and water (CCW) model integrates hydrological and ecological processes by mechanistically linking vegetation dynamics to water and

carbon fluxes through remote sensing-driven parameterization (Li et al., 2024b; Zhang et al., 2021b, 2022b). Unlike the Budyko framework's empirical parameter "n"—which conflates vegetation effects with unaccounted catchment characteristics—the CCW model links vegetation and hydrology through a single mechanistic chain. In this framework, vegetation structure (NDVI/LAI) determines canopy absorption of photosynthetically active radiation (FPAR) and hence gross primary production (GPP) via light-use efficiency, while evapotranspiration (ET) is coupled to GPP through a biome-specific underlying water-use efficiency (UWUE) term with vapor pressure deficit (VPD) regulation.~~CCW explicitly resolves vegetation impacts through two distinct pathways: (1) structural effects—quantified by NDVI-modulated canopy absorption of photosynthetically active radiation (FPAR) that captures changes in energy partitioning due to vegetation greening; and (2) physiological adjustments—represented by biome-specific variations in underlying water-use efficiency (UWUE) and vapor pressure deficit (VPD)-mediated regulation of evapotranspiration (ET). In the model, GPP is estimated from light-use efficiency theory (ε_{pot} × FPAR × PAR× Rs × Ts × Ws), and ET is mechanistically coupled to GPP via UWUE—a physiologically grounded parameter representing ecosystem-level carbon–water trade-offs, calibrated against global FLUXNET observations (Zhang et al., 2016b), which encapsulates ecosystem-level carbon–water trade-offs. By contrast, Budyko's empirical "n" aggregates these distinct vegetation controls into a single catchment-scale parameter, obscuring their individual hydrological impacts.~~

~~-~~Nevertheless, the original CCW model, while robust in capturing vegetation-climate interactions, adopts a static UWUE and does not account for CO_2-induced physiological changes, specifically long-term enhancements in water-use efficiency (WUE) resulting from elevated [CO_2], thereby limiting its capacity to isolate [CO_2] fertilization effects from vegetation structural and climatic influences (Adams et al., 2020; Li et al., 2023).~~This omission limits its ability to isolate [CO_2] fertilization effects from climate and LULC (land use and land cover) changes, a gap particularly~~

~~problematic in regions like China, where CO_2-driven WUE improvements may offset or amplify vegetation greening impacts on runoff.~~

To address this limitation, our study enhanced the CCW framework by incorporating dynamic WUE responses to [CO_2], allowing explicit attribution of runoff changes to three distinct drivers—climate change (eg. precipitation, temperature, and so on), vegetation structural change (NDVI, and land use and land cover (LULC)), and [CO_2]-physiological effects (stomatal optimization).~~Therefore, we aim to improve the CCW model by incorporating dynamic WUE responses to [CO_2], building on the biome-specific UWUE framework.~~ This extension advances beyond empirical or regression-based attribution, clarifies how [CO_2] modulates vegetation–hydrology interactions across large spatial scales, and provides policy-relevant evidence for sustainable water resource management and ecological restoration in China under accelerating environmental change. ~~Furthermore, by integrating CO_2-dependent WUE adjustments into the ET-GPP coupling, our improved model explicitly partitions runoff changes into three causal drivers: (1) climate change (eg. precipitation, temperature, and so on), (2) vegetation structural changes (NDVI, and land use and land cover (LULC)), and (3) CO_2-physiological effects (stomatal optimization)~~.

2 Methods and Data

2.1 Data sources and processing

Four main datasets were employed in the improved CCW model: vegetation data (NDVI), climate data (precipitation, temperature, shortwave radiation, vapor pressure deficit, and atmospheric pressure), land use and land cover (LULC), and [CO_2]. The monthly NDVI dataset used in this study (Table 1) was derived from a daily 0.05° gap-free NDVI dataset in China (https://doi.org/10.6084/m9.figshare.c.7002225.v1) (Li et al., 2024a), which was developed from the NOAA's daily NDVI dataset, applying effective data recognition and spatiotemporal gap-filling techniques. The dataset spans

1981–2023 and provides a spatial resolution of 0.05°, and we used bilinear interpolation to generate the dataset with a spatial resolution of 0.1°.

Climate data (Table 1), including precipitation, air temperature, surface downward shortwave radiation, relative humidity, and atmospheric pressure, were sourced from the China Meteorological Forcing Dataset (CMFD) at the National Tibetan Plateau Data Center (TPDC) of the Institute of Tibetan Plateau Research, Chinese Academy of Sciences (He et al., 2020). The dataset spans 1979–2018 and provides a spatial resolution of 0.1° and temporal resolutions at 3-hour, daily, monthly, and annual scales. As the dataset did not provide vapor pressure deficit (VPD), we calculated VPD using the method from Howell and Dusek (1995), based on atmospheric pressure, temperature, and relative humidity.

LULC data (Table 1) were obtained from the Zhang et al. (2024) global dataset, which provides consistent multi-temporal global LULC maps at 30 m spatial resolution for 1985–2022. The dataset includes 35 fine-resolution LULC types. For the purposes of this study, and to facilitate LULC change analysis, we merged these 35 LULC types into 17 types using the IGBP classification, based on the method by Yang et al. (2017). Four primary LULC types—cropland, forest, grassland, and bare land—were determined following the method described by Mu et al. (2013). The data were resampled to the 0.1° spatial resolution, ensuring compatibility for modeling within the modified CCW framework.

[CO_2] data were sourced from the Mauna Loa Observatory (MLO), Hawaii (20°N, 156°W) (http://cdiac.esd.ornl.gov/ftp/trends/co2/ maunaloa.co2), with yearly observations used to represent national [CO_2] levels due to the minimal spatial variation in [CO_2] across China (Table 1). These datasets were then used to drive the improved CCW model.

In this study, the hydrological data for model validation from 145 hydrological stations (Fig. 1), each with at least 15 years of continuous data since 1982, was collected

from the Hydrological Bureau of the Ministry of Water Resources of China (https://www.mwr.gov.cn/english/). Annual runoff data were calculated from the daily runoff and the catchment area controlled by each hydrological station.

Table 1. Hydrology, climate, and vegetation data for the improved CCW model

Dataset	Original Resolution (spatial/temporal)	Period	Reference
NDVI	0.05° ×0.05° (daily)	1981 - 2023	(Li et al., 2024a)
Landcover	30m×30m (5-year)	1985 - 2022	(Zhang et al., 2024)
Climate	0.1° ×0.1° (monthly)	1979 - 2018	(He et al., 2020)
[CO_2]	yearly	1959 - 2023	Mauna Loa Observatory, Hawaii
Streamflow	daily	1982 - 1995 (or later)	On-site streamflow records and the regional flow summary reports of government

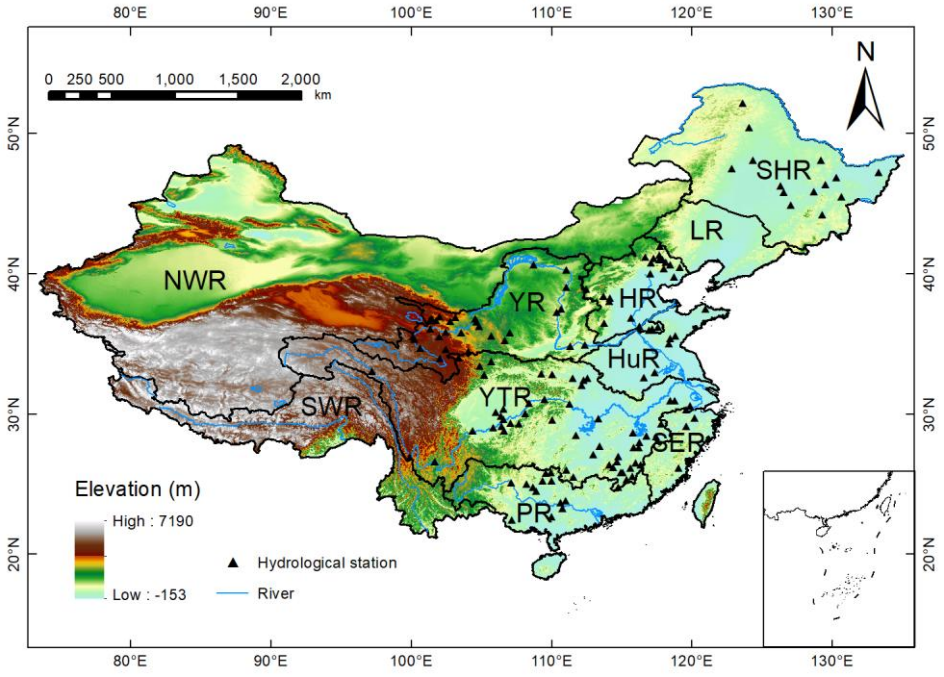

Figure 1. The geographic location and topography of the study area, where the black triangles mark the location of the hydrological gauging stations for model evaluation. Ten river basins considered in this study are: Songhua River basin (SHR), Liao River basin (LR), Hai River basin (HR), Huai River basin (HuR), Yangtze River basin (YZR), Yellow River basin (YR), Pearl River basin (PR), Southeast Rivers (SER), Southwest Rivers (SWR) and Northwest Rivers (NWR).

2.2 The improved CCW model

The original Coupled Carbon and Water (CCW) model (Zhang et al., 2016b) is a data-driven, remote sensing-based model that effectively integrates carbon and water

dynamics to estimate monthly gross primary productivity (GPP) and evapotranspiration (ET). This model, which is particularly carbon-centric, derives ET from GPP constrained by underlying water-use efficiency (UWUE) parameters, which were calibrated using global FLUXNET data (Zhang et al., 2016b; Zhou et al., 2014). Despite its simpler structure, the CCW model achieves accuracy comparable to more complex process-based models in ET estimation. The essential components of the CCW model are represented as:

$$GPP = APAR \times \varepsilon = PAR \times FPAR \times \varepsilon_{pot} \times R_s \times T_s \times W_s \quad (1)$$

where APAR is the absorbed photosynthetically active radiation (MJ m^{-2}), which is calculated as the product of incident photosynthetically active radiation (PAR) and the fraction of PAR absorbed by vegetation (FPAR), and PAR is typically assumed to be 45% of the total shortwave radiation (Running et al., 2000); FPAR is determined by the normalized difference vegetation index (NDVI) (Sims et al., 2005); ε is the realized light-use efficiency (g C MJ^{-1}), which is calculated by multiplying the potential light-use efficiency (ε_{pot}) and environmental scalars for diffuse radiation (Rs), temperature (Ts), and moisture stress (Ws). This formulation ensures that GPP estimates reflect the influence of radiation, temperature, and moisture limitations on photosynthetic activity.

In this study, we improve the CCW model by incorporating dynamic water use efficiency (WUE) instead of static UWUE. This enhancement addresses the limitations of the original model, particularly its inability to adapt to environmental changes such as varying [CO_2] and vapor pressure deficit (VPD). WUE's estimation method is estimated using the WEC (Water Efficiency and Carbon) equation proposed by Cheng et al. (2017). The final formula for calculating WUE is:

$$WUE = \frac{C_a \times P_a}{1.6\left(VPD + g_1\sqrt{VPD}\right)}[1 - exp(-k * LAI)](1 - f_i) \quad (2)$$

where C_a is atmospheric CO_2 concentration (mol(CO_2) mol^{-1}(air)); Pa is atmospheric pressure (kPa); VPD is vapor pressure deficit (kPa); g_1 is an empirical parameter of the Ball stomatal conductance model; k is the radiation extinction coefficient, typically set

at 0.6, describing how light is absorbed by the canopy; LAI is the leaf area index; and f_i is a factor representing nonproductive water use (such as evaporation from soil and canopy interception). This equation provides a dynamic estimate of WUE, considering the effects of environmental factors like VPD, CO_2 concentration, atmospheric pressure, and canopy structure (LAI). The factor 1−exp(−k×LAI) accounts for light interception by the canopy. In this study, the interception evaporation factor (f_i) was set to zero. This simplification follows previous large-scale ecohydrological studies (Cheng et al., 2017), which reported that canopy interception and soil surface evaporation account for a minor portion of total evapotranspiration at annual to multi-decadal scales. Given that the improved CCW model focused on yearly water yield (WY) dynamics rather than event-scale hydrological responses, neglecting interception loss reduces model complexity without substantially affecting WY estimation.

In order to ensure the consistency of NDVI and LAI trends, we calculated LAI using NDVI (Gutman and Ignatov, 1998) instead of LAI dataset:

$$\begin{cases} LAI = -2ln(1 - f_{NDVI}) \\ f_{NDVI} = \dfrac{NDVI - NDVI_0}{NDVI_1 - NDVI_0} \end{cases} \quad (3)$$

where $NDVI_0 = 0.04$, $NDVI_1 = 0.52$

Evapotranspiration (ET) is then calculated as the ratio of GPP to WUE:

$$ET = \frac{GPP}{WUE} \quad (4)$$

This modification allows the model to estimate ET using dynamic WUE, replacing the static UWUE from the original model. The dynamic nature of WUE enhances the model's ability to simulate ecosystem water use across different environmental conditions and vegetation types.

Finally, the water yield (WY) is calculated as the difference between precipitation (P) and ET:

$$WY = P - ET \quad (5)$$

On an annual scale, WY is assumed to be approximately equal to runoff, as changes in soil water storage over long periods (one year or longer) are considered negligible (Xiao et al., 2020; Zhang et al., 2021b). Thus, the attribution of WY can also be considered as the attribution of runoff. Accordingly, in this study WY is used as the modelled output, while the term 'runoff' is reserved for observed streamflow or literature values explicitly labelled as such.

2.3 Attribution analysis framework

To explore the combined and individual effects of climate, vegetation, and [CO_2] change on water yield (WY), four scenarios were designed based on data from 1982 to 2017 (Table 2). Scenario 1 (Actual) aimed to validate the improved CCW model and estimate the combined effects of climate, vegetation, and [CO_2] change on WY by allowing all variables to vary from 1982 to 2017. Scenario 2 (Vegetation Change) focused on estimating the direct effects of vegetation change on WY by allowing vegetation variables (NDVI and LULC) to vary while keeping climate and [CO_2] fixed at 1982 levels. In this case, the trend in WY obtained reflects the impact of vegetation change alone. Scenario 3 (Climate Change) aimed to estimate the direct effects of climate change on WY by allowing climate variables (precipitation, temperature, relative humidity, solar radiation, and atmospheric pressure) to change, while fixing vegetation and [CO_2] at 1982 levels. This scenario helps isolate the effects of climate change on WY. Scenario 4 ([CO_2] Change) was designed to estimate the direct effects of [CO_2] change on WY by varying [CO_2] levels from 1982 to 2017, while climate and vegetation variables were fixed at 1982 levels. The resulting WY trend reflects the impact of [CO_2] change alone. The resulting WY series under each scenario represents the isolated impact of the corresponding driver.

Table 2. Scenario designs in the improved CCW model for WY attribution. LULC: Land use and land cover types; NDVI: Normalized difference vegetation index; TMP: Temperature; SRAD: Shortwave radiation; VPD: Vapor pressure deficit.

Scenarios	Vegetation		Climate					CO_2	Purposes
	LULC	NDVI	P	T	RH	Srad	Pa	CO_2	
S1 (baseline)	▲	▲	▲	▲	▲	▲	▲	▲	Validating the improved CCW model and estimating the combined effects of climate, vegetation, and CO_2 change.
S2 (vegetation)	▲	▲	△	△	△	△	△	△	Estimating the direct effects of vegetation change.
S3 (climate)	△	△	▲	▲	▲	▲	▲	△	Estimating the direct effects of climate change.
S4 (CO_2)	△	△	△	△	△	△	△	▲	Estimating the direct effects of CO_2 change.

Note: The symbol "▲" denotes a changing input variable over time, whereas the symbol "△" represents a fixed input variable at the level of the initial year (1982).

For each scenario, the long-term trend in annual WY over 1982–2017 was quantified using the Theil–Sen estimator, yielding a robust slope. The relative contributions of climate, vegetation, and [CO_2] to changes in WY were calculated using the following formula (Ma et al., 2023; Wang et al., 2022):

$$\begin{cases} RC_{vegetation} = \dfrac{trend_{vegetation}}{|trend_{vegetation}| + |trend_{climate}| + |trend_{CO2}|} \times 100\% \\ RC_{climate} = \dfrac{trend_{climate}}{|trend_{vegetation}| + |trend_{climate}| + |trend_{CO2}|} \times 100\% \\ RC_{CO2} = \dfrac{trend_{CO2}}{|trend_{vegetation}| + |trend_{climate}| + |trend_{CO2}|} \times 100\% \end{cases} \quad (6)$$

where $trend_{vegetation}$, $trend_{climate}$, and $trend_{CO2}$ represent the changes in water yield (WY) resulting from vegetation, climate, and [CO_2] changes, respectively, as calculated in each scenario; the relative contributions ($RC_{vegetation}$, $RC_{climate}$, and

RC_{CO2}) are expressed as percentages, indicating the proportion of each factor's influence on the overall changes in WY.

At each grid point, the absolute values of the relative contributions of each factor (vegetation, climate, and [CO_2]) are compared. For each grid point, we identify the most significant contributor to water yield (WY) changes by comparing the relative contributions of each factor. If the absolute values of the relative contributions of two factors do not exceed 5%, then these two factors are considered joint significant contributors to the changes in WY at that grid point ~~(Ma et al., 2024; Saltelli et al., 2007)~~ (Jia et al., 2022). This approach helps to highlight areas where the impacts of multiple factors are closely intertwined and both play a critical role in influencing water yield, suggesting that their combined effects are comparable in magnitude. In these cases, the relative contribution of each factor is not significantly stronger than the other, indicating that their combined influence on WY is equally important at the local scale.

The scenario analysis previously conducted revealed the relative contributions of climate, vegetation, and [CO_2] to WY changes. However, these contributions arise from both the intrinsic rate of change of each factor and the sensitivity of runoff to those changes (the elasticity coefficient) (Yang and Yang, 2011). To gain a deeper understanding of the changes in WY, we employ elasticity coefficients to quantify its sensitivity to individual factor. We specifically focused on precipitation because, despite not always having the highest sensitivity, it is integral to the hydrological cycle and essential for assessing water yield (WY) under various climate change scenarios (Liu et al., 2017). The elasticity of runoff refers to the variation in runoff depth resulting from a 1% increase in each climatic variable (Xu et al., 2014). The absolute value of elasticity reflects the sensitivity of runoff to various influencing factors. In other methods, elasticity coefficients are typically calculated using an analytical expression based on instantaneous changes in runoff corresponding to variations in a given factor in a specific year (Fu et al., 2023; Liu et al., 2017; Yang and Yang, 2012). However, in our study, we applied scenario-based analysis over the period of 1982 to 2017. This

extended temporal window allowed us to better account for the long-term effects and interactions of multiple factors influencing WY. So we vary each factor (precipitation, NDVI, and [CO_2]) by 1% relative to the baseline scenario S1 across the entire 1982-2017 period. We then calculated the annual average runoff values from the adjusted sequence and compared them with the average original baseline runoff values. The difference between these two values, divided by the average baseline runoff value, gave us the runoff change rate:

$$\frac{\Delta R_x}{R_x} = \frac{WY_{mean_x} - WY_{mean_x}}{WY_{mean_x}} \quad (7)$$

Mathematically, the elasticity coefficient is defined as the runoff change rate divided by 1%, and the formula is as follows:

$$\varepsilon_x = \frac{\frac{\Delta R_x}{R_x}}{\frac{\Delta x}{x}} = \frac{\frac{\Delta R_x}{R_x}}{1\%} \quad (8)$$

Generally, while the scenario analysis above has identified which factors are most influential based on their relative contributions, the elasticity coefficients allow us to explain why these factors are critical by demonstrating their respective impacts on WY through sensitivity analysis. This dual approach—combining both the changes in the factors and their elasticities—provides a more comprehensive understanding of the drivers behind the observed changes in WY, ensuring that the results of the scenario analysis are both meaningful and robust.

3 Results

3.1 Changes in hydrometeorological variables

Fig. 2 demonstrates the trends of annual precipitation, air temperature, relative humidity, atmospheric pressure, solar radiation, and NDVI across China during 1982-2017. Annual precipitation change exhibited a clear spatial distribution pattern, specifically decreases in central China, including the middle reaches of the Yellow

River and the Yangtze River basins, and increases in the northwest and southeast. Air temperature exhibited a consistent warming trend across China. In contrast, relative humidity generally decreased across most China. Atmospheric pressure remained relatively stable. Regarding solar radiation, decreases were in northern China, while an increase was in southern regions. The decreasing solar radiation in northern China is likely due to increased aerosol concentrations (Liang et al., 2024). NDVI showed a significant increasing trend, which indicates an overall enhancement in vegetation growth across China. This trend was especially prominent in central and eastern regions, including the Yellow River Basin and the Yangtze River Basin. In these regions, LULC changes, such as afforestation and agricultural practices, likely contributed to the observed increases in NDVI (Chen et al., 2019).

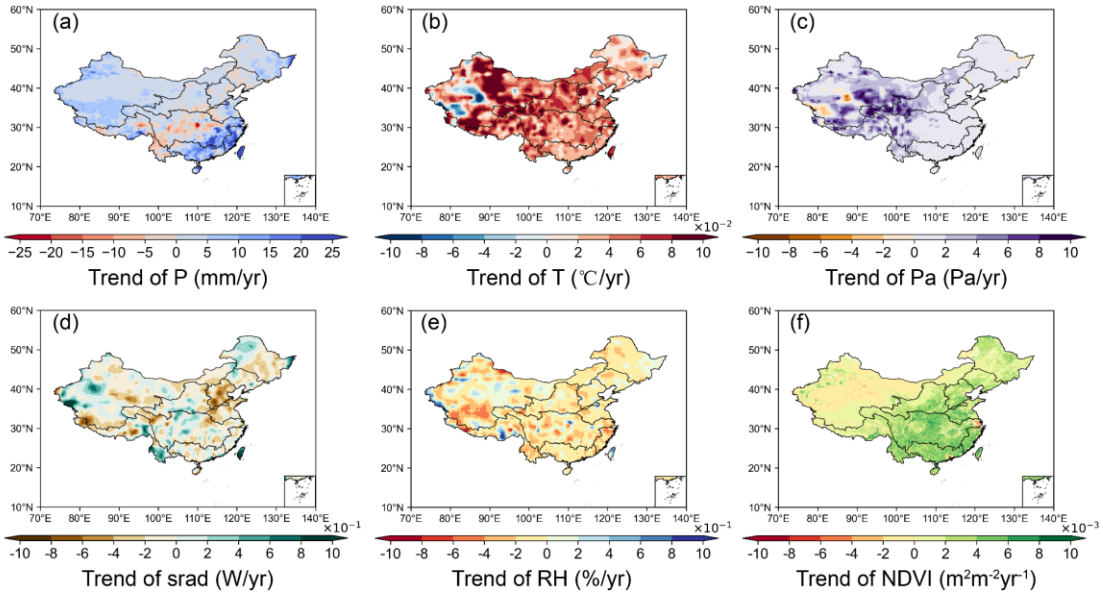

Figure 2. Spatial patterns of trends in annual climatic and vegetation variables during 1982–2017. (a) precipitation (mm/yr); (b) air temperature (°C/yr); (c) Atmospheric pressure (Pa/yr); (d) shortwave radiation (W/m^2/yr); (e) relative humidity (%/yr); (f) NDVI (yr^{-1}).

Significant changes in land use and land cover (LULC) occurred in China during 1982-2017, as illustrated in Fig. 3. Although the overall percentage distribution of major land cover types, namely grasslands, forests, croplands, and bare lands, remained relatively stable, these four categories dominated the landscape, with most changes concentrated within them. Notably, the transitions among these categories were

characterized by mutual conversions, particularly from bare land to grasslands (Fig. 3). Spatially, the changes exhibited distinct regional patterns. In southern China, LULC changes were mainly characterized by the conversion of land to forests and grasslands. In contrast, the northeastern regions exhibited more complex transformations, with some areas shifting to bare land and croplands (Fig. 3).

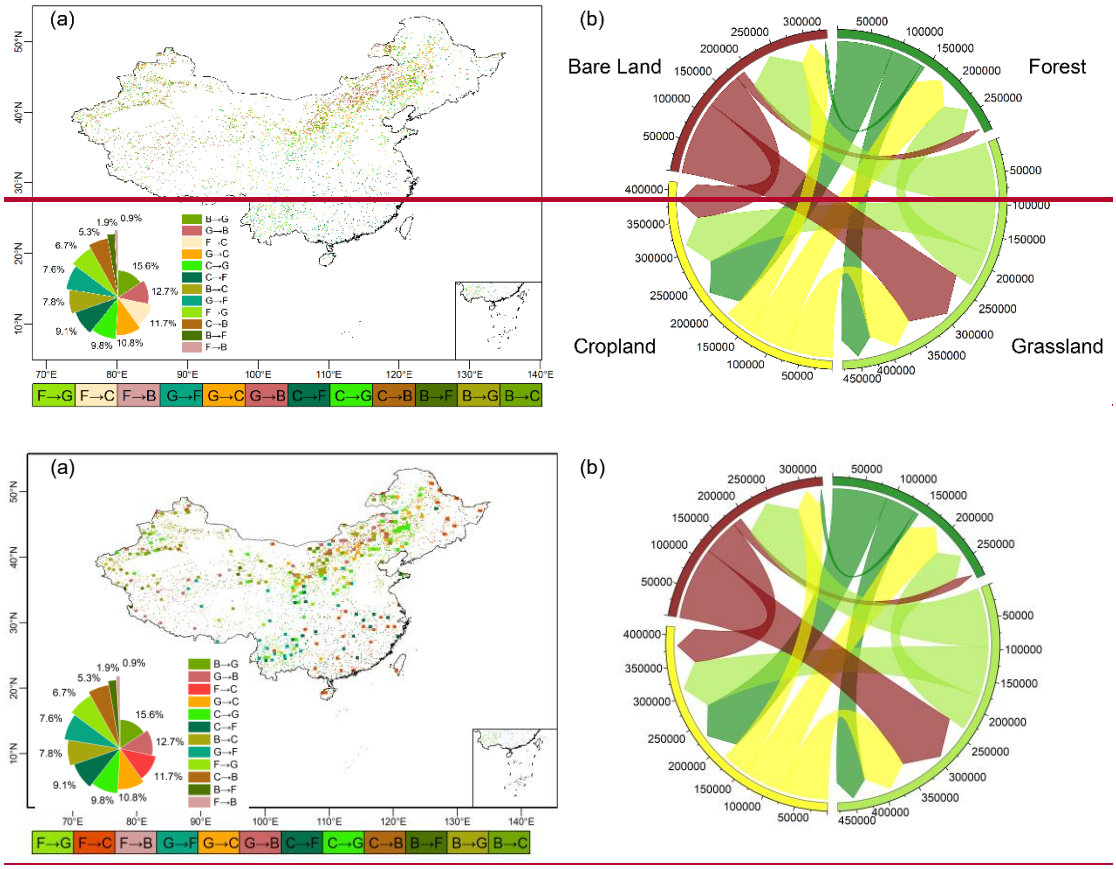

Figure 3. Land use and land cover (LULC) changes from 1982 to 2017. (a) Spatial pattern distribution of LULC change; (b) Chord diagram of LULC conversion flows (unit: km^2), where directional arrows represent transitions between land types (originating type → current type), with chord widths proportional to the converted areas. The figure illustrates the converted areas and does not include the unchanged regions.

3.2 Performance of the improved CCW model

As shown in Fig. 4a and b, the observed annual water yield (WY) and the simulated annual WY by the improved CCW model showed strong linear correlations (R^2 = 0.7), with the regression line slope being 1.45, R^2 being 0.7, and RMSE being 9.54 mm/year. By contrast, the initial model without WUE showed weaker skill (slope

= 1.45 , R^2 = 0.68, RMSE = 9.62 mm·yr^{-1}), indicating that explicitly representing [CO_2]-induced regulation of water-use efficiency measurably improves accuracy and reduces bias.~~It indicates that the model provides a reliable representation of the observed trends.~~

The estimated annual WY trends had distinct spatial patterns (Fig. ~~4b~~4c), which closely aligned with that of precipitation. Specifically, decrease trends in WY occurred in the central regions of the Yellow River Basin and the middle section of the Yangtze River Basin, while increase trends were found in other regions, with the southeast exhibiting the highest rate of increase.

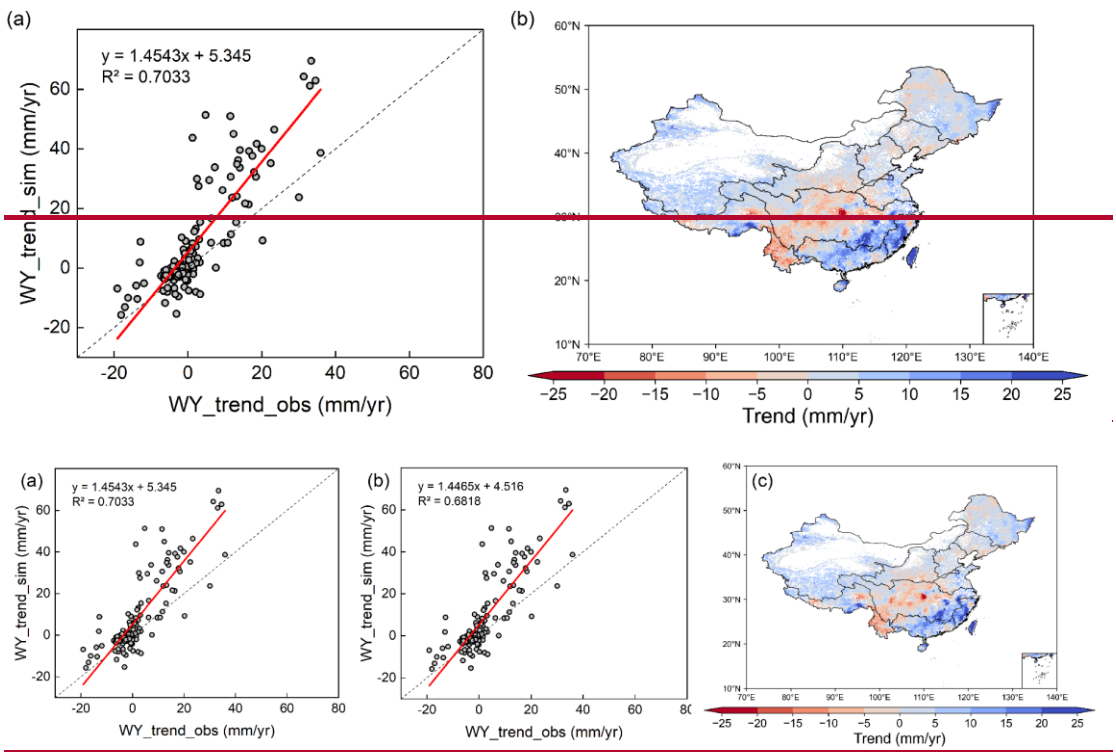

Figure 4. (a) Validation of simulated WY trend using the improved CCW model; (b) Validation of simulated WY trend using the initial CCW model; (~~b~~c) Spatial distribution of WY trends under scenario S1(actual situation) during 1982–2017.

3.3 Attribution analysis of annual WY changes

Fig. 5 shows the distribution of WY changes caused by climate, vegetation, and [CO_2] changes, integrating both absolute magnitude (Fig. 5a-c) and relative dominance (Fig. 5d-f) of their contributions. Climate-driven WY changes exhibited marked spatial heterogeneity, with absolute increases exceeding 15 mm/yr in southeastern China (Fig.

5a), corresponding to 60-90% relative contributions (Fig. 5d). Central basins showed contrasting declines of 0-6 mm/yr under climate forcing, while northeastern transitional zones displayed mixed positive/negative absolute changes (Fig. 5a) despite maintaining 40-70% relative climate dominance (Fig. 5d). This spatial heterogeneity aligned with precipitation change patterns (Fig. 2a).

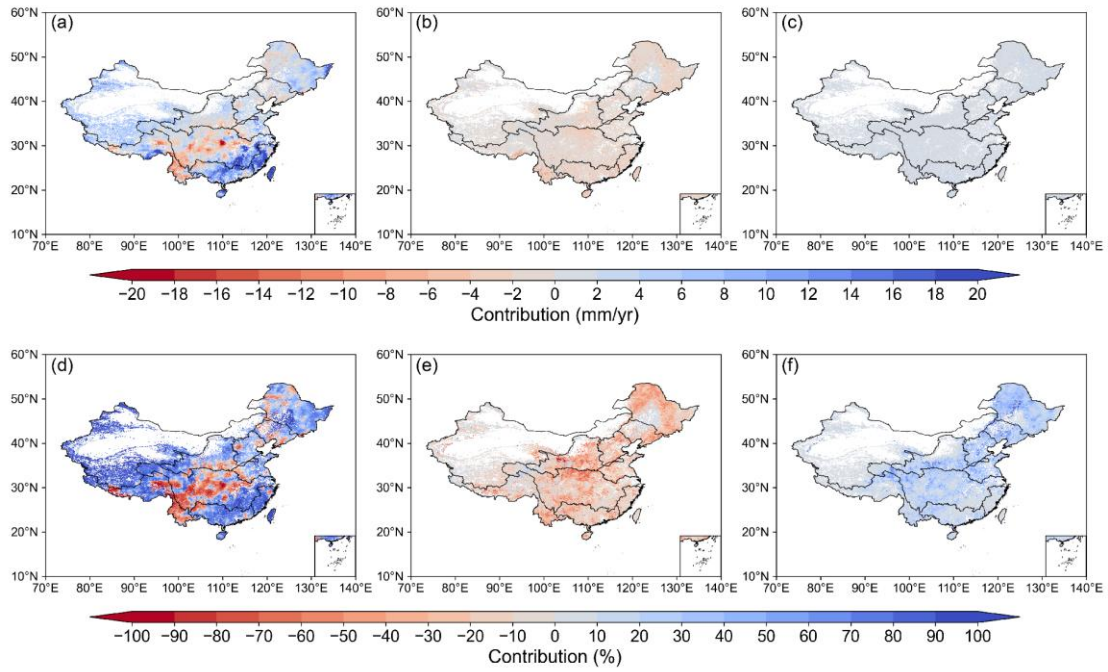

Figure 5. The absolute contributions of (a) climate, (b) vegetation, and (c) [CO_2], and the relative contributions of (d) climate, (e) vegetation, and (f) [CO_2] to changes in WY trends for 1982-2017.

Vegetation-mediated WY reductions reached 0-6 mm/yr (Fig. 5b), accompanied by 0-60% relative contributions (Fig. 5e). These effects originated from enhanced evapotranspiration through land-use changes and NDVI-based greening, particularly pronounced in central China. Specific regions in the Yangtze, Yellow, and northeastern rivers showed vegetation-driven relative contributions reaching 40-60% (Fig. 5e). [CO_2] effects generated limited direct absolute impacts (<5 mm/yr, Fig. 5c) but exerted 10-40% relative influences (Fig. 5f) through stomatal closure mechanisms. This process partially counteracted vegetation-related WY losses in transitional climates like northeastern China, where competing drivers created complex ecohydrological interactions (Fig. 5d-f).

Fig. 6 illustrated the spatial distribution of WY trend drivers over the past four decades. Climate change was the dominant factor of WY variation in more than 70% regions, mainly in the Northwest, Southwest, Southeast, Pearl River basins, and other parts of the Yangtze and Yellow River basins. Vegetation changes ranked as the secondary control, dominating WY changes in parts of the Yangtze, Yellow, Songhua, Liao, and Hai Rivers. Remarkably, it was shown that the region where vegetation and [CO_2] had the dominant influence mainly distributes within precipitation ranges of 400–1600 mm. CO_2-induced effects were least influential at a national scale. This three-tiered hierarchy—climate changes as the primary forcing, vegetation changes as the secondary control, and [CO_2] effects as a localized modifier—reveals how hydrological regimes govern the spatial succession of dominant drivers across China's diverse ecohydrological gradients.

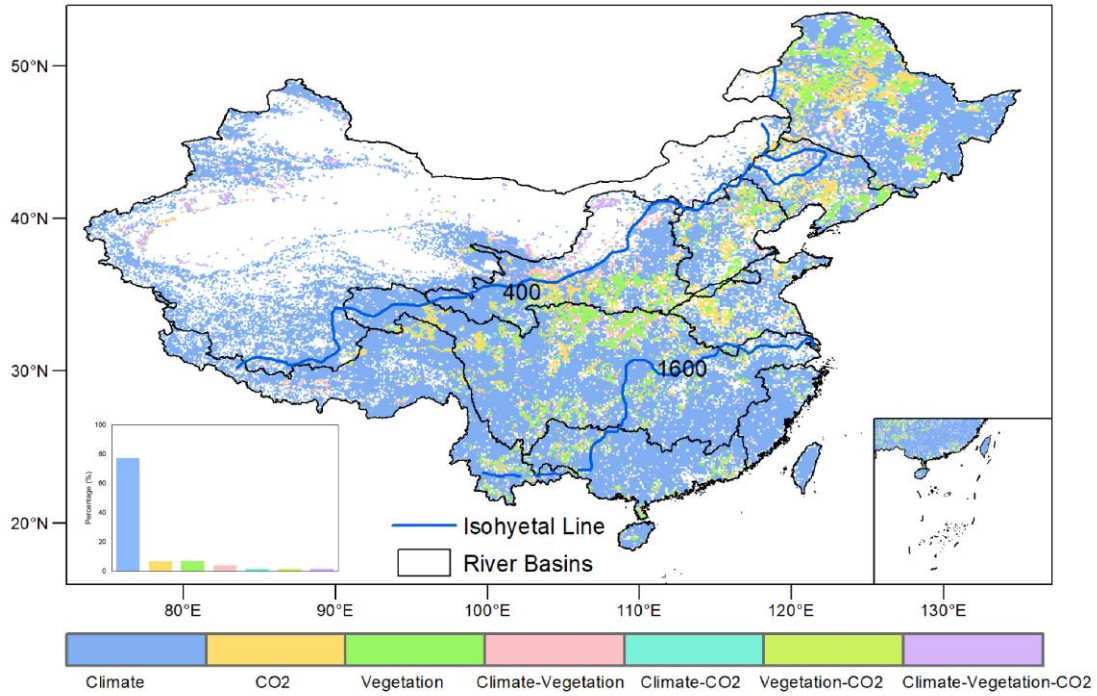

Figure 6. Spatial distributions of dominant factors controlling WY change. Driving factors include climate, vegetation, and [CO_2]. Climate: Areas where climate (e.g., precipitation, temperature) is the dominant factor influencing WY change; CO2: Areas where [CO_2] is the primary driver of WY change; Vegetation: Areas where vegetation changes (e.g., NDVI, LULC) primarily drive WY changes. Climate-Vegetation: Areas where both climate and vegetation jointly influence WY; Climate-CO2: Areas where both climate and [CO_2] jointly contribute to WY change; Vegetation-CO2: Areas where vegetation changes and [CO_2] jointly

control WY; Climate-Vegetation-CO2: Areas where the combined effect of climate, vegetation, and [CO_2] jointly controls WY change. Additionally, the approximate isohyetal line shown in the figure were derived based on annual precipitation data from 1982 to 2017.

3.4 Elasticity of WY to main variables

The sensitivity of WY to precipitation (εP), NDVI (εNDVI), and [CO_2] (εCO_2) exhibits distinct spatial patterns in (Fig. 7). Nationally averaged elasticity coefficients showed that a 10% increase in precipitation, [CO_2], and NDVI altered WY by 15.5% (εP=1.55), 5.5% (εCO_2=0.55), and -4.4% (εNDVI=-0.44), respectively, indicating that, in terms of the sensitivity of runoff to changes in each factor, the ranking was precipitation > [CO_2] > NDVI.

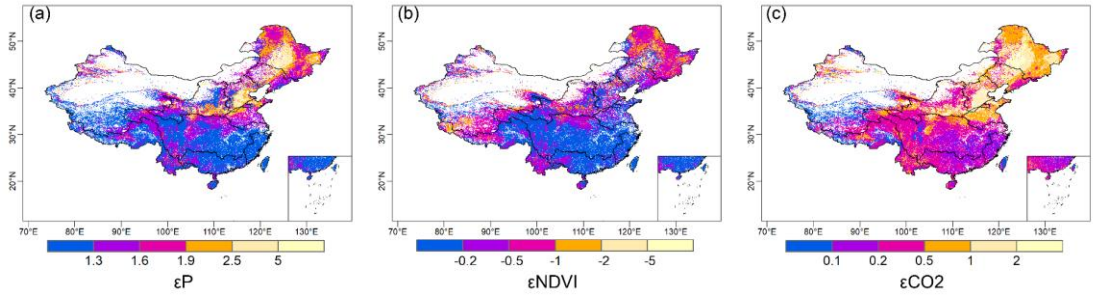

Figure 7. Spatial distribution of elasticity coefficients of WY relative to changes in hydrological variables such as (a) annual precipitation, (b) NDVI, and (c) [CO_2].

The elasticity coefficients of precipitation (εP), [CO_2] (εCO_2), and vegetation (|εNDVI|) all exhibited a coherent latitudinal decline across China's river basins, showing systematically higher sensitivity in northern regions than southern counterparts. Quantitatively, εP decreased from 2.09 in the Songhua River basin to 1.15 in the Southeastern Basin, accompanied by similar reductions in |εNDVI| (from 0.76 to 0.13) and εCO_2 (from 1.08 to 0.16) (Table 3).

A distinct abrupt transition zone in elasticity coefficients was identified around 33°N, closely aligning with China's traditional North-South physiographic divide. Around the zone, elasticity coefficients exhibited an abrupt decline from the Yellow River Basin to the Yangtze River Basin. Specifically, the Yellow River Basin showed higher sensitivities to precipitation (εP=1.87), [CO_2] (εCO_2=0.86), and NDVI

(εNDVI=-0.53), which were approximately 1.4, 2.8, and 2.8 times greater, respectively, than those in the Yangtze River Basin (εP=1.31, εCO_2=0.31, εNDVI=-0.19).

Table 3. Elasticity Coefficients of Runoff to Precipitation, NDVI, and CO_2 in Different Watersheds

Dataset	εP	εNDVI	εCO_2
Songhua River basin	2.09	-0.76	1.08
Hai River basin	2.13	-0.44	1.12
Yellow River basin	1.87	-0.53	0.86
Yangtze River Basin	1.31	-0.19	0.31
Huai River basin	1.64	-0.18	0.63
Pearl River basin	1.25	-0.17	0.25
Southeast Rivers	1.15	-0.13	0.15

Note: Some LULC types were excluded from the analysis. Due to many missing data points, the Liao River, Southwest, and Northwest river basins were also omitted.

4 Discussion

4.1 Strength of the attribution analysis framework

To address limitations in current methods for analysing the effects of climate, vegetation, and [CO_2] on runoff changes, we developed an attribution analysis framework based on the improved CCW model. This framework has been improved in three aspects. Firstly, the explicit and mechanistic integration of vegetation dynamics and [CO_2] effects overcomes the oversimplifications inherent in conventional approaches. Traditional Budyko-based frameworks often attribute vegetation effects to temporal variations in the parameter "n" by either statistically regressing "n" against vegetation proxies such as NDVI (Liu et al., 2024; Tan et al., 2023) or simplistically equating "n" to vegetation effects (Li et al., 2020b; Zhou et al., 2023). Such approaches conflate structural vegetation changes (e.g., leaf area index) with physiological adjustments (e.g., CO_2-induced stomatal closure), thereby obscuring the independent roles of vegetation dynamics and [CO_2]. For example, while rising [CO_2] levels directly reduce stomatal conductance and transpiration, Budyko-based studies often misinterpret this effect as part of the "n" parameter's variability, erroneously attributing

it to vegetation changes (Zeng et al., 2020). In contrast, our framework mechanistically separates these pathways by explicitly describing the stomatal conductance–WUE relationship based on plant physiological theory. Elevated [CO_2] reduces stomatal aperture, thereby lowering stomatal conductance and transpiration flux while only modestly increasing carbon assimilation, leading to an overall enhancement in water-use efficiency (WUE). This process is represented by the Medlyn-type stomatal conductance model (Medlyn et al., 2011), which links photosynthetic rate (A), transpiration (T), and vapor pressure deficit (D) as:

$$\frac{A}{T} = \frac{C_a P_a}{1.6\left(D + g_1\sqrt{D}\right)}$$

where C_a is atmospheric CO_2 concentration, P_a is air pressure, D is vapor pressure deficit, and g_1 is an empirical slope parameter that quantifies plant sensitivity to CO_2 and humidity. According to this formulation, rising [CO_2] increases while reducing stomatal conductance, which in turn suppresses transpiration more strongly than photosynthesis, resulting in higher WUE. This mechanistic representation enables our framework to capture the direct physiological CO_2 effect on evapotranspiration, which is otherwise masked in Budyko-type models where CO_2 impacts are embedded implicitly in PET or the "n" parameter.

~~: structural modifications are distinguished from CO_2-driven stomatal physiological responses, resolving contradictions in prior findings where vegetation greening was reported to both mitigate (Zeng et al., 2018) and exacerbate (Farley et al., 2005) runoff changes.~~

Secondly, unlike Budyko-based methods that indirectly represent [CO_2] impacts through adjustments to potential evapotranspiration (PET)—a practice conflating [CO_2] effects with meteorological drivers like radiation and wind—our framework explicitly quantifies CO_2's physiological influence on actual evapotranspiration (AET) by mechanistically modeling its role in stomatal conductance and water-use efficiency (WUE). Elevated [CO_2] reduces stomatal conductance and transpiration while

moderately enhancing carbon assimilation, partially offsetting water losses associated with vegetation greening.~~Elevated [CO_2] reduces stomatal aperture, directly suppressing transpiration while enhancing carbon assimilation.~~ For example, our results show that reduction in transpiration due to CO_2-driven stomatal closure offsets water losses, a mechanism entirely masked in Budyko frameworks where [CO_2] effects are ambiguously embedded in PET adjustments or erroneously attributed to vegetation structural changes via the "n" parameter (Liu et al., 2024). This coupled regulation clarified how water and energy jointly constrain evapotranspiration, particularly in 400-1600 mm precipitation zones. In these regions, vegetation growth enhanced transpiration and root water uptake until increasing atmospheric aridity imposed physiological constraints, while rising [CO_2] partially counteracted this effect by improving water-use efficiency through stomatal closure. As a result, the framework provided a more mechanistically grounded understanding of how CO_2 fertilization modulates ecosystem water use and hydrological responses at regional scales.

Thirdly, while numerous studies have conducted runoff attribution analysis at the basin scale (Liu et al., 2024, 2017; Yang et al., 2022), our grid-scale approach transcends the spatial constraints of fixed watershed boundaries by resolving regional heterogeneity in hydrological drivers. Conventional basin-aggregated methods obscure critical intra-basin differences—for instance, our analysis reveals that grids in the upper Yangtze River basin, where precipitation change dominates runoff trends, necessitate climate scenario-based water resource planning. In contrast, mid-basin grids with significant NDVI-driven greening exhibit pronounced WY reductions, highlighting the need for vegetation management strategies that restrict excessive afforestation in water-sensitive areas (Sun et al., 2022; Yang et al., 2021). By decoupling analysis from rigid watershed boundaries, our framework enables targeted strategies such as restricting reforestation in water-stressed grids or selecting CO_2-adapted vegetation species, thereby aligning management actions with localized climate-vegetation-hydrology interactions.

4.2 New insights into attribution analysis

Our findings highlighted climate change as the dominant driver of water yield (WY) changes (contributing >70%), consistent with other assessments (Table 4), yet reveal critical regional divergences. Climate impacts dominated in the Northwest and Southwest River Basins, as well as parts of the Yangtze, Yellow, Southeast, and Pearl River Basins, while vegetation and [CO_2] effects prevailed in central China (parts of the Yangtze, Yellow, Songhua, Liao, and Hai River basin)—a spatial pattern slightly distinct from earlier studies. Although previous studies identified human activities as the primary driver in some northern basins (Liao, Hai, and Yellow River Basins) ((Yang et al., 2022), their long-term study (1965-2018) diluted the gradually strengthening vegetation signals after 2000 mentioned in other studies (Liu et al., 2017; Sun et al., 2023) through time-averaging. Our findings now confirm the emerging importance of vegetation dynamics in southern basins like the Yangtze through our symmetric 1982-2017 study period.

Table 4. Comparative studies of the contribution of climate variability and vegetation to runoff changes.

Reference	Study region	Study period	Method/Model	Driving factors
(Wei et al., 2024)	Global	1981-2020	Trendy phase 11 +ROF	Climate change
(Liu et al., 2024)	Global	1984-2010; 2000-2100	Improved Budyko	Precipitation
(Zhou et al., 2023)	Global	1850-2014; 2015-2100	Improved Budyko + CMIP6	Land surface changes
(Tan et al., 2023)	Global	2003-2016; 1982-2016	Improved Budyko	Effective precipitation
(Yang et al., 2022)	China	1965-2018	Budyko	P: Northwest river basin, Southwest river basin, Yangtze river basin, Southeast river basin, and Pearl river basin; n: Liaohe river basin, Haihe river basin, Yellow river Basin, Songhuajiang river basin, and Huaihe river basin
(Zhang et al., 2022b)	Yangtze River	2001-2018	CCW Model	Climate variability
(Chen et al., 2022)	Six river basins in China	1982-2015	Gray Relational Analysis (GRA)	Precipitation

(Zhai and Tao, 2021)	China	1982-2015	VIC Model	Climate change
(Li et al., 2020a)	Yihe River	1960-2013	SWAT+WRF	Climate variability
(Shen et al., 2017)	China	1960-2010	Budyko	Underlying surface change (n): the Songhua Basin, the Liaohe Basin and the Haihe Basin; Climate change: in other basins.

Elasticity analysis (Section 3.4) revealed distinct sensitivities of WY to environmental drivers: precipitation exhibited the highest elasticity coefficient for the whole China ($\varepsilon P = 1.55$), followed by CO_2 ($\varepsilon CO_2 = 0.55$) and NDVI ($\varepsilon NDVI = -0.44$). However, spatial analysis showed that vegetation and [CO_2] collectively dominated WY changes in 400–1600 mm/yr precipitation zones, despite their lower sensitivity rankings. ~~This apparent contradiction stemmed from the interplay between elasticity and the magnitude of driver change.~~ The joint effect of elasticity and the magnitude of driver change that determines each driver's net contribution. In the 400–1600 mm/yr precipitation zones, NDVI displayed ~~high spatial heterogeneity~~ (Fig. 8) a larger relative temporal variation compared with precipitation, which fluctuated within a narrower range.~~whereas precipitation fluctuated within a narrower relative range~~. Consequently, vegetation's stronger relative change~~spatiotemporal variability~~ amplified its hydrological influence, overriding its lower elasticity. Similarly, CO_2's historical impact was constrained by its slow accumulation rate (0.49%/yr), yet its relatively high elasticity positions it as a latent driver.

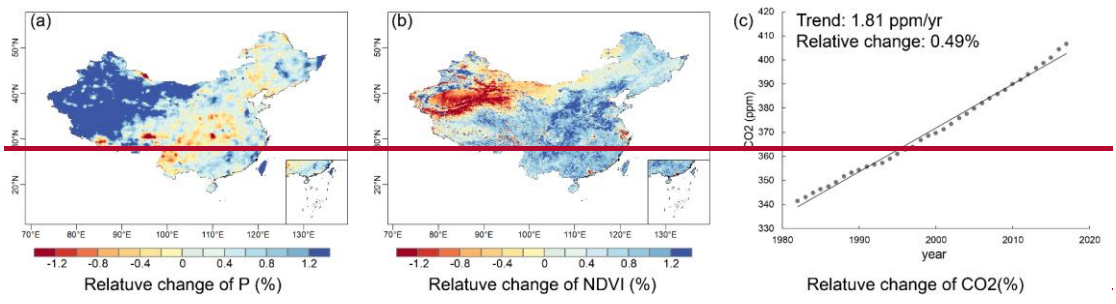

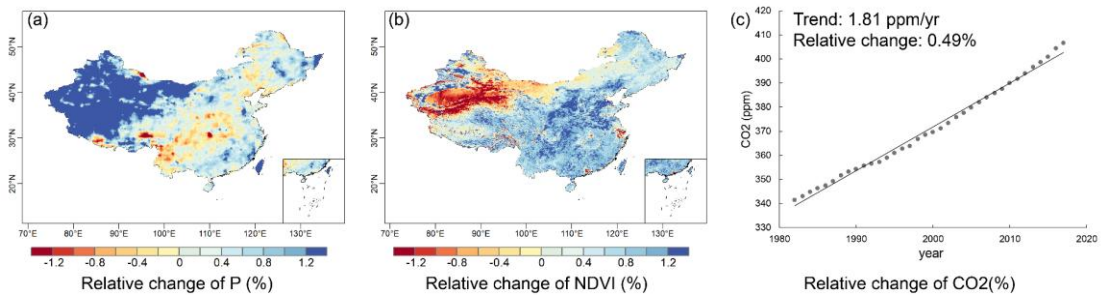

Figure 8. Spatial distribution of relative changes of different variables: (a) annual precipitation, and (b) NDVI.

This historical constraint, however, belied CO_2's transformative potential under intensified forcing scenarios. CMIP6 SSP585 projections indicate [CO_2] will rise at 2.34%/yr—nearly fivefold faster than historical rates (Cheng et al., 2022). At this trajectory, CO_2's elasticity would drive a +1.29% annual WY increase, eclipsing both vegetation greening effects and even surpassing precipitation-driven changes in some regions. Such reversal underscores the imperative to prioritize [CO_2] in long-term water management, particularly in 400–1600 mm/yr precipitation zones.

From a policy perspective, these spatial contrasts have distinct implications for regional water management. In vegetation-dominated regions such as the Yangtze and Huang river basins, enhancing ecosystem-based restoration, optimizing vegetation composition, and preventing overgreening that may suppress runoff should be prioritized. Conversely, in climate-dominated areas such as Northwest and Southeast China, adaptive measures emphasizing precipitation variability, water storage capacity, and drought resilience are crucial. Recognizing and tailoring water management strategies to these driver-specific regimes can enhance the effectiveness of both ecological restoration and climate adaptation programs across China.

4.3 Uncertainty in attribution analysis

This study provides valuable insights into the relationship between water resources management and environmental changes, which can guide environmental management

strategies. However, several limitations exist that need to be addressed in future work to improve the accuracy and robustness of the results.

Firstly, the improved CCW model does not account for the variation and specific values of f_i, assuming f_i is 0. In reality, f_i represents the ratio of interception evaporation to total evaporation, and in regions with abundant vegetation, f_i is not zero. Despite this, considering the small change of f_i in the current year (Zhao et al., 2022), its influence on runoff trends is negligible in our study (Cheng et al., 2017). However, future work should prioritize its calculation to improve the precision of WY estimates.

Secondly, the complex interrelationships among climate, vegetation, and [CO_2] cannot be fully disentangled. Vegetation exhibits tight biophysical interactions and feedback with climate, making it difficult to separate the impacts of climate change, vegetation dynamics, and [CO_2] on hydrological responses. Changes in vegetation, such as NDVI, reflect a combination of climate change, human activities (e.g., reforestation and irrigation), and natural vegetation growth. Additionally, vegetation greening in upwind regions can increase atmospheric moisture, potentially enhancing precipitation downwind (Zhang et al., 2021a), which may counteract some of the negative impacts of increased evapotranspiration on local WY. Although the climate data used in our model may implicitly capture some of these feedbacks, they cannot be explicitly separated in this analysis. Consequently, our results represent an attempt to estimate the direct first-order net impacts of climate, vegetation greening, and [CO_2] increase on WY (Zhang et al., 2021b). Future research should adopt more comprehensive models that consider soil-vegetation-atmosphere interactions to better differentiate the contributions of each driving factor to WY.

Thirdly, the improved CCW model does not incorporate certain human activities, such as large-scale irrigation, groundwater pumping, and reservoir regulation~~dam construction and water extraction~~, which should be incorporated in future studies. For instance, irrigation can sustain vegetation greening during dry seasons, potentially amplifying the vegetation–climate feedback on water yield. Incorporating such

anthropogenic processes into the CCW framework through coupled irrigation and water management modules would enable more comprehensive attribution analyses in future studies. Our research also excludes water bodies and built-up land. While urbanization can increase flood risks due to the growing proportion of impervious surfaces (Wasko and Sharma, 2017), these land-use changes represent a small portion of China's land area.

Finally, the future impact of vegetation greening on hydrological dynamics will depend on projected climate warming and drying trends, the persistence of vegetation greening, [CO_2] changes, and the complex feedbacks between climate, soil, and vegetation. These interactions require long-term study, and future research will involve more extensive monitoring to better capture these evolving dynamics.

5 Conclusions

In this study, we improved the CCW model incorporating dynamic water use efficiency (WUE) calculation to explicitly represent CO_2-physiological feedback on water yield. This mechanistic improvement enabled comprehensive national-scale assessment quantifying the relative contributions of climate forcing, vegetation structural changes, and CO_2-driven stomatal regulation to water yield (WY) dynamics in China. The main conclusions are as follows:

The improved CCW model effectively simulated WY variations in most basins under increased [CO_2] scenarios, demonstrating its applicability and reliability in modeling WY changes.

Climate change, particularly variations in precipitation, emerged as the primary driver influencing WY, displaying significant regional disparities in its effects. Vegetation changes constituted the second most critical factor, predominantly resulting in WY reduction, notably in central China. While the effect of CO_2-induced stomatal closure on WY was comparatively minor. Spatial analysis aligned with isohyetal lines

further revealed that vegetation change and [CO_2] exerted greater influence within the 400–1600 mm precipitation range.

The elasticity analysis of WY indicated that northern basins exhibit higher sensitivity to influencing factors, whereas southern basins demonstrate relatively lower elasticity. Specifically, the absolute elasticity coefficients for the whole China were ranked in descending order as follows: precipitation > [CO_2] > NDVI. Thus, accelerating [CO_2] rise (2.34% /yr under SSP585) will amplify its hydrological role, potentially elevating CO_2-driven WY increases to +1.29% annually by 2100, surpassing climate and vegetation impacts.

These insights provide a nuanced understanding of regional hydrological responses, essential for sustainable water resource management under changing environmental conditions.

Acknowledgements

This research was supported by the China National Key R&D Program (grant no. 2024YFF1306901).

Data Availability Statement

Datasets used for driving models were obtained from different sources described in Table 1. All the data related to our results in this study can be found online: the NDVI data (https://doi.org/10.6084/m9.figshare.c.7002225.v1); the climate data (https://www.tpdc.ac.cn/zh-hans/data/8028b944-daaa-4511-8769-965612652c49/); the land use and land cover (LULC) data (https://zenodo.org/records/8239305) (Liu et al., 2023); and the [CO_2] (http://cdiac.esd.ornl.gov/ftp/trends/co2/maunaloa.co2), except for the streamflow records for hydrological gauging stations, which are available upon reasonable request.

Author contributions

HS designed the study, developed the model code, did the simulation experiments, and wrote the first draft of the paper. HY designed the research and edited the manuscript. CL provided feedback on the results and edited the manuscript.

Competing interests

The contact author has declared that neither they nor their co-authors have any competing interests.

Reference

Adams, M. A., Buckley, T. N., and Turnbull, T. L.: Diminishing CO2-driven gains in water-use efficiency of global forests, Nat. Clim. Chang., 10, 466–471, https://doi.org/10.1038/s41558-020-0747-7, 2020.

Chen, C., Park, T., Wang, X., Piao, S., Xu, B., Chaturvedi, R. K., Fuchs, R., Brovkin, V., Ciais, P., Fensholt, R., Tømmervik, H., Bala, G., Zhu, Z., Nemani, R. R., and Myneni, R. B.: China and India lead in greening of the world through land-use management, Nat Sustain, 2, 122–129, https://doi.org/10.1038/s41893-019-0220-7, 2019.

Chen, S., Fu, Y. H., Geng, X., Hao, Z., Tang, J., Zhang, X., Xu, Z., and Hao, F.: Influences of Shifted Vegetation Phenology on Runoff Across a Hydroclimatic Gradient, Front. Plant Sci., 12, 802664, https://doi.org/10.3389/fpls.2021.802664, 2022.

Cheng, L., Zhang, L., Wang, Y.-P., Canadell, J. G., Chiew, F. H. S., Beringer, J., Li, L., Miralles, D. G., Piao, S., and Zhang, Y.: Recent increases in terrestrial carbon uptake at little cost to the water cycle, Nat Commun, 8, 110, https://doi.org/10.1038/s41467-017-00114-5, 2017.

Cheng, W., Dan, L., Deng, X., Feng, J., Wang, Y., Peng, J., Tian, J., Qi, W., Liu, Z., Zheng, X., Zhou, D., Jiang, S., Zhao, H., and Wang, X.: Global monthly gridded atmospheric carbon dioxide concentrations under the historical and future scenarios, Sci Data, 9, 83, https://doi.org/10.1038/s41597-022-01196-7, 2022.

Fu, J., Liu, B., Wang, W., and Fei, E. X.: Evaluating main drivers of runoff changes across China from 1956 to 2000 by using different budyko-based elasticity methods, Journal of Environmental Management, 329, 117070, https://doi.org/10.1016/j.jenvman.2022.117070, 2023.

Gan, G., Liu, Y., and Sun, G.: Understanding interactions among climate, water, and vegetation with the Budyko framework, Earth-Science Reviews, 212, 103451, https://doi.org/10.1016/j.earscirev.2020.103451, 2021.

Gutman, G. and Ignatov, A.: The derivation of the green vegetation fraction from NOAA/AVHRR data for use in numerical weather prediction models, International Journal of Remote Sensing, 19, 1533–1543, https://doi.org/10.1080/014311698215333, 1998.

He, J., Yang, K., Tang, W., Lu, H., Qin, J., Chen, Y., and Li, X.: The first high-resolution meteorological forcing dataset for land process studies over China, Sci Data, 7, 25, https://doi.org/10.1038/s41597-020-0369-y, 2020.

Howell, T. A. and Dusek, D. A.: Comparison of Vapor-Pressure-Deficit Calculation Methods—Southern High Plains, J. Irrig. Drain Eng., 121, 191–198, https://doi.org/10.1061/(ASCE)0733-9437(1995)121:2(191), 1995.

Jia, Y., Li, C., Yang, H., Yang, W., and Liu, Z.: Assessments of three evapotranspiration products over China using extended triple collocation and water balance methods, Journal of Hydrology, 614, 128594, https://doi.org/10.1016/j.jhydrol.2022.128594, 2022.

Jiao, Y., Lei, H., Yang, D., Huang, M., Liu, D., and Yuan, X.: Impact of vegetation dynamics on hydrological processes in a semi-arid basin by using a land surface-hydrology coupled model, Journal of Hydrology, 551, 116–131, https://doi.org/10.1016/j.jhydrol.2017.05.060, 2017.

Lammertsma, E. I., Boer, H. J. D., Dekker, S. C., Dilcher, D. L., Lotter, A. F., and Wagner-Cremer, F.: Global CO_2 rise leads to reduced maximum stomatal conductance in Florida vegetation, Proc. Natl. Acad. Sci. U.S.A., 108, 4035–4040, https://doi.org/10.1073/pnas.1100371108, 2011.

Li, B., Shi, X., Lian, L., Chen, Y., Chen, Z., and Sun, X.: Quantifying the effects of climate variability, direct and indirect land use change, and human activities on runoff, Journal of Hydrology, 584, 124684, https://doi.org/10.1016/j.jhydrol.2020.124684, 2020a.

Li, F., Xiao, J., Chen, J., Ballantyne, A., Jin, K., Li, B., Abraha, M., and John, R.: Global water use efficiency saturation due to increased vapor pressure deficit, Science, 381, 672–677, https://doi.org/10.1126/science.adf5041, 2023.

Li, H., Shi, C., Zhang, Y., Ning, T., Sun, P., Liu, X., Ma, X., Liu, W., and Collins, A. L.: Using the Budyko hypothesis for detecting and attributing changes in runoff to climate and vegetation change in the soft sandstone area of the middle Yellow River basin, China, Science of The Total Environment, 703, 135588, https://doi.org/10.1016/j.scitotenv.2019.135588, 2020b.

Li, H., Cao, Y., Xiao, J., Yuan, Z., Hao, Z., Bai, X., Wu, Y., and Liu, Y.: A daily gap-free normalized difference vegetation index dataset from 1981 to 2023 in China, Sci Data, 11, 527, https://doi.org/10.1038/s41597-024-03364-3, 2024a.

Li, X., Xu, X., Sonnenborg, T. O., Andreasen, M., and He, C.: Effect of ecological restoration on evapotranspiration and water yield in the agro-pastoral ecotone in northern China during 2000–2018, Journal of Hydrology, 638, 131531, https://doi.org/10.1016/j.jhydrol.2024.131531, 2024b.

Liang, L., Han, Z., Chen, W., Li, J., Liang, M., and Shen, S.: The source, transport, deposition and direct radiative effect of mineral dust over western China: A modeling

study of July 2022 with focus on the Tibetan Plateau, Atmospheric Research, 311, 107708, https://doi.org/10.1016/j.atmosres.2024.107708, 2024.

Liu, C., Feng, S., Zhang, Q., Hu, J., Ma, N., Ci, H., Kong, D., and Gu, X.: Critical influence of vegetation response to rising CO2 on runoff changes, Science of The Total Environment, 906, 167717, https://doi.org/10.1016/j.scitotenv.2023.167717, 2024.

Liu, J., Zhang, Q., Singh, V. P., and Shi, P.: Contribution of multiple climatic variables and human activities to streamflow changes across China, Journal of Hydrology, 545, 145–162, https://doi.org/10.1016/j.jhydrol.2016.12.016, 2017.

Ma, T., Wang, T., Yang, D., and Yang, S.: Impacts of vegetation restoration on water resources and carbon sequestration in the mountainous area of Haihe River basin, China, Science of The Total Environment, 869, 161724, https://doi.org/10.1016/j.scitotenv.2023.161724, 2023.

Medlyn, B. E., Duursma, R. A., Eamus, D., Ellsworth, D. S., Prentice, I. C., Barton, C. V. M., Crous, K. Y., De Angelis, P., Freeman, M., and Wingate, L.: Reconciling the optimal and empirical approaches to modelling stomatal conductance: RECONCILING OPTIMAL AND EMPIRICAL STOMATAL MODELS, Global Change Biology, 17, 2134–2144, https://doi.org/10.1111/j.1365-2486.2010.02375.x, 2011.

Montibeller, B., Marshall, M., Mander, Ü., and Uuemaa, E.: Increased carbon assimilation and efficient water usage may not compensate for carbon loss in European forests, Commun Earth Environ, 3, 194, https://doi.org/10.1038/s43247-022-00535-1, 2022.

Mu, S., Zhou, S., Chen, Y., Li, J., Ju, W., and Odeh, I. O. A.: Assessing the impact of restoration-induced land conversion and management alternatives on net primary productivity in Inner Mongolian grassland, China, Global and Planetary Change, 108, 29–41, https://doi.org/10.1016/j.gloplacha.2013.06.007, 2013.

Nkiaka, E., Bryant, R. G., and Dembélé, M.: Quantifying Sahel Runoff Sensitivity to Climate Variability, Soil Moisture and Vegetation Changes Using Analytical Methods, Earth Syst Environ, 9, 491–504, https://doi.org/10.1007/s41748-024-00464-3, 2025.

Ogutu, B. O., D'Adamo, F., and Dash, J.: Impact of vegetation greening on carbon and water cycle in the African Sahel-Sudano-Guinean region, Global and Planetary Change, 202, 103524, https://doi.org/10.1016/j.gloplacha.2021.103524, 2021.

Peng, H., Tague, C., and Jia, Y.: Evaluating the eco-hydrologic impacts of reforestation in the Loess Plateau, China, using an eco-hydrologic model, Ecohydrology, 9, 498–513, https://doi.org/10.1002/eco.1652, 2016.

Piao, S., Friedlingstein, P., Ciais, P., De Noblet-Ducoudré, N., Labat, D., and Zaehle, S.: Changes in climate and land use have a larger direct impact than rising CO_2 on global river runoff trends, Proc. Natl. Acad. Sci. U.S.A., 104, 15242–15247, https://doi.org/10.1073/pnas.0707213104, 2007.

Rahman, G., Farooq, U., Jung, M.-K., and Kwon, H.-H.: Spatiotemporal vegetation dynamics in South Asia (2001-2023): roles of climate and anthropogenic activities, Geosci. Lett., 12, 31, https://doi.org/10.1186/s40562-025-00403-8, 2025.

Running, S. W., Thornton, P. E., Nemani, R., and Glassy, J. M.: Global Terrestrial Gross and Net Primary Productivity from the Earth Observing System, in: Methods in Ecosystem Science, edited by: Sala, O. E., Jackson, R. B., Mooney, H. A., and Howarth, R. W., Springer New York, New York, NY, 44–57, https://doi.org/10.1007/978-1-4612-1224-9_4, 2000.

Serrano-Notivoli, R., Martínez-Salvador, A., García-Lorenzo, R., Espín-Sánchez, D., and Conesa-García, C.: Rainfall–runoff relationships at event scale in western Mediterranean ephemeral streams, Hydrol. Earth Syst. Sci., 26, 1243–1260, https://doi.org/10.5194/hess-26-1243-2022, 2022.

Shen, Q., Cong, Z., and Lei, H.: Evaluating the impact of climate and underlying surface change on runoff within the Budyko framework: A study across 224 catchments in China, Journal of Hydrology, 554, 251–262, https://doi.org/10.1016/j.jhydrol.2017.09.023, 2017.

Sims, D. A., Rahman, A. F., Cordova, V. D., Baldocchi, D. D., Flanagan, L. B., Goldstein, A. H., Hollinger, D. Y., Misson, L., Monson, R. K., Schmid, H. P., Wofsy, S. C., and Xu, L.: Midday values of gross CO2 flux and light use efficiency during satellite overpasses can be used to directly estimate eight-day mean flux, Agricultural and Forest Meteorology, 131, 1–12, https://doi.org/10.1016/j.agrformet.2005.04.006, 2005.

Sun, W., Ding, X., Su, J., Mu, X., Zhang, Y., Gao, P., and Zhao, G.: Land use and cover changes on the Loess Plateau: A comparison of six global or national land use and cover datasets, Land Use Policy, 119, 106165, https://doi.org/10.1016/j.landusepol.2022.106165, 2022.

Sun, X., Dong, Q., and Zhang, X.: Attribution analysis of runoff change based on Budyko-type model with time-varying parameters for the Lhasa River Basin, Qinghai–Tibet Plateau, Journal of Hydrology: Regional Studies, 48, 101469, https://doi.org/10.1016/j.ejrh.2023.101469, 2023.

Tan, X., Tan, X., Liu, B., and Huang, Z.: Contribution of changes in vegetation composition and climate variability on streamflow across the global watersheds, CATENA, 232, 107394, https://doi.org/10.1016/j.catena.2023.107394, 2023.

880 Tan, X., Jia, Y., Yang, D., Niu, C., and Hao, C.: Impact ways and their contributions to
881 vegetation-induced runoff changes in the Loess Plateau, Journal of Hydrology:
882 Regional Studies, 51, 101630, https://doi.org/10.1016/j.ejrh.2023.101630, 2024.

883 Wang, D. L., Feng, H. M., Zhang, B. Z., Wei, Z., and Tian, Y. L.: Quantifying the
884 impacts of climate change and vegetation change on decreased runoff in china's yellow
885 river basin, Ecohydrology & Hydrobiology, 22, 310–322,
886 https://doi.org/10.1016/j.ecohyd.2021.10.002, 2022.

887 Wasko, C. and Sharma, A.: Global assessment of flood and storm extremes with
888 increased temperatures, Sci Rep, 7, 7945, https://doi.org/10.1038/s41598-017-08481-1,
889 2017.

890 Wei, H., Zhang, Y., Huang, Q., Chiew, F. H. S., Luan, J., Xia, J., and Liu, C.: Direct
891 vegetation response to recent CO2 rise shows limited effect on global streamflow, Nat
892 Commun, 15, 9423, https://doi.org/10.1038/s41467-024-53879-x, 2024.

893 Xiao, M., Gao, M., Vogel, R. M., and Lettenmaier, D. P.: Runoff and
894 Evapotranspiration Elasticities in the Western United States: Are They Consistent With
895 Dooge's Complementary Relationship?, Water Resources Research, 56,
896 e2019WR026719, https://doi.org/10.1029/2019WR026719, 2020.

897 Xu, X., Yang, D., Yang, H., and Lei, H.: Attribution analysis based on the Budyko
898 hypothesis for detecting the dominant cause of runoff decline in Haihe basin, Journal
899 of Hydrology, 510, 530–540, https://doi.org/10.1016/j.jhydrol.2013.12.052, 2014.

900 Xu, Z., Jiang, Y., Jia, B., and Zhou, G.: Elevated-CO2 Response of Stomata and Its
901 Dependence on Environmental Factors, Front. Plant Sci., 7,
902 https://doi.org/10.3389/fpls.2016.00657, 2016.

903 Xue, B., A, Y., Wang, G., Helman, D., Sun, G., Tao, S., Liu, T., Yan, D., Zhao, T.,
904 Zhang, H., Chen, L., Sun, W., and Xiao, J.: Divergent Hydrological Responses to Forest
905 Expansion in Dry and Wet Basins of China: Implications for Future Afforestation
906 Planning, Water Resources Research, 58, e2021WR031856,
907 https://doi.org/10.1029/2021WR031856, 2022.

908 Yang, H. and Yang, D.: Derivation of climate elasticity of runoff to assess the effects
909 of climate change on annual runoff: DERIVATION OF CLIMATE ELASTICITY OF
910 RUNOFF, Water Resour. Res., 47, https://doi.org/10.1029/2010WR009287, 2011.

911 Yang, H. and Yang, D.: Climatic factors influencing changing pan evaporation across
912 China from 1961 to 2001, Journal of Hydrology, 414–415, 184–193,
913 https://doi.org/10.1016/j.jhydrol.2011.10.043, 2012.

914 Yang, H., Xu, H., Huntingford, C., Ciais, P., and Piao, S.: Strong direct and indirect
915 influences of climate change on water yield confirmed by the Budyko framework,
916 Geography and Sustainability, 2, 281–287,
917 https://doi.org/10.1016/j.geosus.2021.11.001, 2021.

918 Yang, L., Zhao, G., Tian, P., Mu, X., Tian, X., Feng, J., and Bai, Y.: Runoff changes in
919 the major river basins of China and their responses to potential driving forces, Journal
920 of Hydrology, 607, 127536, https://doi.org/10.1016/j.jhydrol.2022.127536, 2022.

921 Yang, Y., Xiao, P., Feng, X., and Li, H.: Accuracy assessment of seven global land
922 cover datasets over China, ISPRS Journal of Photogrammetry and Remote Sensing, 125,
923 156–173, https://doi.org/10.1016/j.isprsjprs.2017.01.016, 2017.

924 Yang, Y., Roderick, M. L., Zhang, S., McVicar, T. R., and Donohue, R. J.: Hydrologic
925 implications of vegetation response to elevated CO2 in climate projections, Nature
926 Clim Change, 9, 44–48, https://doi.org/10.1038/s41558-018-0361-0, 2019.

927 Zeng, F., Ma, M.-G., Di, D.-R., and Shi, W.-Y.: Separating the Impacts of Climate
928 Change and Human Activities on Runoff: A Review of Method and Application, Water,
929 12, 2201, https://doi.org/10.3390/w12082201, 2020.

930 Zhai, R. and Tao, F.: Climate Change in China Affects Runoff and Terrestrial
931 Ecosystem Water Retention More Than Changes in Leaf Area Index and Land
932 Use/Cover Over the Period 1982–2015, JGR Biogeosciences, 126, e2020JG005902,
933 https://doi.org/10.1029/2020JG005902, 2021.

934 Zhang, B., Tian, L., Zhao, X., and Wu, P.: Feedbacks between vegetation restoration
935 and local precipitation over the Loess Plateau in China, Sci. China Earth Sci., 64, 920–
936 931, https://doi.org/10.1007/s11430-020-9751-8, 2021a.

937 Zhang C., WU C., KUAI S., PENG Z., Chang R., and ZHANG S.: Water-heat coupling
938 model-based study on runoff driving mechanism of Zhenjiangguan Watershed, Water
939 Resources and Hydropower Engineering, 53, 78–87,
940 https://doi.org/10.13928/j.cnki.wrahe.2022.08.008, 2022a.

941 Zhang, J., Zhang, Y., Sun, G., Song, C., Dannenberg, M. P., Li, J., Liu, N., Zhang, K.,
942 Zhang, Q., and Hao, L.: Vegetation greening weakened the capacity of water supply to
943 China's South-to-North Water Diversion Project, Hydrol. Earth Syst. Sci., 25, 5623–
944 5640, https://doi.org/10.5194/hess-25-5623-2021, 2021b.

945 Zhang, J., Zhang, Y., Sun, G., Song, C., Li, J., Hao, L., and Liu, N.: Climate Variability
946 Masked Greening Effects on Water Yield in the Yangtze River Basin During 2001–
947 2018, Water Resources Research, 58, e2021WR030382,
948 https://doi.org/10.1029/2021WR030382, 2022b.

Zhang, S., Yang, H., Yang, D., and Jayawardena, A. W.: Quantifying the effect of vegetation change on the regional water balance within the Budyko framework, Geophysical Research Letters, 43, 1140–1148, https://doi.org/10.1002/2015GL066952, 2016a.

Zhang, X., Zhao, T., Xu, H., Liu, W., Wang, J., Chen, X., and Liu, L.: GLC_FCS30D: the first global 30 m land-cover dynamics monitoring product with a fine classification system for the period from 1985 to 2022 generated using dense-time-series Landsat imagery and the continuous change-detection method, Earth Syst. Sci. Data, 16, 1353–1381, https://doi.org/10.5194/essd-16-1353-2024, 2024.

Zhang, Y., Song, C., Sun, G., Band, L. E., McNulty, S., Noormets, A., Zhang, Q., and Zhang, Z.: Development of a coupled carbon and water model for estimating global gross primary productivity and evapotranspiration based on eddy flux and remote sensing data, Agricultural and Forest Meteorology, 223, 116–131, https://doi.org/10.1016/j.agrformet.2016.04.003, 2016b.

Zhao, F., Wu, Y., Ma, S., Lei, X., and Liao, W.: Increased Water Use Efficiency in China and Its Drivers During 2000–2016, Ecosystems, 25, 1476–1492, https://doi.org/10.1007/s10021-021-00727-4, 2022.

Zhou, S., Yu, B., Huang, Y., and Wang, G.: The effect of vapor pressure deficit on water use efficiency at the subdaily time scale, Geophysical Research Letters, 41, 5005–5013, https://doi.org/10.1002/2014GL060741, 2014.

Zhou, S., Yu, B., Lintner, B. R., Findell, K. L., and Zhang, Y.: Projected increase in global runoff dominated by land surface changes, Nat. Clim. Chang., 13, 442–449, https://doi.org/10.1038/s41558-023-01659-8, 2023.